Dissolution Arrest and Stability of Particle-Covered Bubbles

Manouk Abkarian,[1,*] Anand Bala Subramaniam,[1] Shin-Hyun Kim,[2] Ryan J. Larsen,[1] Seung-Man Yang,[2] and Howard A. Stone[1,†]

[1]*School of Engineering and Applied Sciences, Harvard University, Pierce Hall, 29 Oxford Street, Cambridge, Massachusetts 02138, USA*

[2]*Center for Integrated Optofluidic Systems and Department of Chemical and Biomolecular Engineering, Korea Advanced Institute of Science and Technology, Daejeon, 305-701, Korea*

(Received 20 December 2006; revised manuscript received 4 July 2007; published 31 October 2007)

Experiments show that bubbles covered with monodisperse polystyrene particles, with particle to bubble radius ratios of about 0.1, evolve to form faceted polyhedral shapes that are stable to dissolution in air-saturated water. We perform SURFACE EVOLVER simulations and find that the faceted particle-covered bubble represents a local minimum of energy. At the faceted state, the Laplace overpressure vanishes, which together with the positive slope of the bubble pressure-volume curve, ensures phase stability. The repulsive interactions between the particles cause a reduction of the curvature of the gas-liquid interface, which is the mechanism that arrests dissolution and stabilizes the bubbles.

DOI: 10.1103/PhysRevLett.99.188301 PACS numbers: 82.70.Dd, 82.70.Rr, 47.55.D−, 68.03.−g

It is well established that colloidal particles adsorbed on bubble surfaces (armored bubbles) can increase bubble [1–4] and foam [5,6] lifetimes by several orders of magnitude in gas-saturated solutions. This increase in stability has applications in fields as diverse as biomedicine [7], materials science [8], mineral flotation [9], and food processing [10]. Nevertheless, in spite of the many reports of long-lived foams and bubbles covered with particles, the mechanism for the stabilization remains an open question.

In this Letter we address the issue of stabilization using both experimental and numerical approaches. We begin by considering the dissolution of a single component gas bubble in a liquid saturated with the same gas. The driving force for dissolution is the pressure difference inside the bubble due to the mean curvature H and the surface tension γ that exists at the bubble surface. This Laplace pressure difference, $\Delta P = 2\gamma H$, is positive for spherical bubbles, and the bubble is thus unstable to dissolution. On thermodynamic grounds, dissolution in saturated solutions can be slowed down if this overpressure is reduced or even stopped if the overpressure is eliminated. As we show below, the stability of armored bubbles, which adopt various nonspherical and irregular shapes in gas-saturated liquid, can be understood in terms of the local geometry of the liquid-gas interface as characterized by the mean and Gaussian curvatures at the scale of individual particles.

We note that several studies provide insight into the relevant particle-interface configurations. For example, numerical studies of fluid infiltration of an infinite packing of spheres on a plane have determined the equilibrium shape of the gas-liquid interface as a function of the contact angle of the particles [11]. The corresponding stability of the interface was addressed in [12], while a 2D analytical study of armored bubbles, including dissolution, found that the ''particles'' pack into a circular shape, while the interface becomes flat [13]. These studies suggest a possible link between bubble stability, the particle configuration, and the equilibrium shape of the fluid-fluid interface.

We perform experiments with negatively charged, surfactant-free fluorescent latex particles (Interfacial Dynamics). Partially coated bubbles were produced as described in [14]. An aqueous sample containing the bubbles was placed on a microscope slide and viewed with an inverted microscope. The small size of the sample ensures that it is saturated with gas. All experiments were carried out at room temperature and repeated at least 3 times. Images were acquired with a CCD camera and treated with Image J to obtain a projection of the visible surface of the armored bubble (for details, see [15]).

In a typical experiment, the particles adsorbed on a partially covered bubble (i.e., the particles are not close packed) are dispersed and exhibit thermal motion [Fig. 1(a)]. Occasionally, a few particles form transient aggregates. Analogous equilibrium configurations of colloidal particles on liquid droplets of fixed volume have been observed [16]. In the case of dissolving gas bubbles, the interparticle distances become smaller until Brownian motion is arrested. This ''jammed'' state can also be reached by packing the bubble surface with colloidal particles in a microfluidic device [17], by fusing two or more particle-covered bubbles [18], by removing a small amount of volume from a particle-covered oil droplet [19] and through the coarsening of a bicontinuous phase [20]. Even after the particle movements have stopped, the bubble continues to lose gas and deforms away from a spherical shape [Fig. 1(a)] before eventually stabilizing. It is this nonspherical bubble that remains stable to further dissolution.

Furthermore, we observe that in air-saturated solutions the final nonspherical shape obtained depends on the ratio of the radius a of the particles and R of the bubble. Bubbles with $a/R \ll 0.1$ appear crumpled when they stabilize [Fig. 1(b)]. Crumpled shapes were apparently first reported

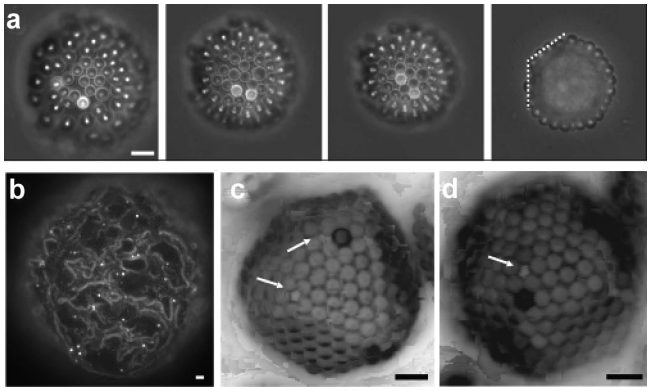

FIG. 1. (a) Experimental images of dissolution of a partially covered bubble, 3 s between each frame. Interparticle distances are reduced and the bubble develops planar facets as it stabilizes (white dashed lines). (b)–(d) Various stable crumpled and faceted shapes of armored bubbles, a/R: (b) 0.008, (c) 0.19, (d) 0.22. The white arrows indicate missing particle defects at the vertices of the bubble. Bubble shapes like these remain stable for days if not longer. Scale bars 8 μm.

by Ramsden [1]; see also, for example, [6,19]. However, for bubbles with $a/R \approx 0.1$, we observe faceted polyhedral structures [Fig. 1(c) and 1(d)], which as far as we know have not been reported in the literature. We observe that the intersection of the facets is a fivefold disclination and is often unoccupied by a particle [white arrows in Fig. 1(c) and 1(d)]. Note that $a/R \approx 1$ corresponds to clusters of particles which have been studied experimentally [21] and via simulations [22].

To gain insight into these particle-covered systems we perform SURFACE EVOLVER (SE) [23] simulations following [22]. We focus on the regime where $a/R \approx 0.1$, and here we report results for a bubble covered with 122 particles ($a/R \approx 0.13$). For verification of reproducibility, including results for larger number of particles, see [15].

Particles of volume V_p are modeled as fluid droplets embedded on a larger fluid droplet (the bubble) of volume V. We define the reduced volume as V/V_p. We chose the particle surface tension (nondimensional) to be 30 times larger than the bubble surface tension. The particles thus remain essentially spherical [22], while the bubble interface is free to evolve as the simulation proceeds. A particle contact angle of 40 degrees was implemented based on previously reported measurements [24]. To further approximate the solid particles, an exponential repulsive potential is introduced in order to ensure particle noninterpenetrability (see [15]). Since large-scale rearrangements are rare close to the jamming transition, we restrict the interparticle potential calculation to nearest neighbors and next nearest neighbors which makes tractable the simulations with large numbers of particles. To approximate the volume reduction that accompanies dissolution, the volume V of the bubble is decreased by 2% decrements in each numerical step. SE calculates the equilibrium configuration of the particles and the shape of the gas-liquid surface at each step by minimizing the sum of the gas-liquid surface energies and the total repulsive energy between the particles.

The simulated armored bubble evolves from a spherical shape [Fig. 2(a)1] towards a polyhedral shape with facets as the reduced volume V/V_p is decreased [Fig. 2(a)2], which is consistent with our experimental observations. Large volume reductions lead to the inward buckling of the facets [indicated by the black arrow in Fig. 2(a)3]. To quantify these observations we calculate the asphericity of the bubble [25], which measures the deviation of the shape from that of a sphere. The asphericity is defined as $\overline{\Delta R^2}/\bar{R}^2 = 1/(N\bar{R}^2)\sum_{i=1}^{N}(R_i - \bar{R})^2$, where N is the number of particles, R_i the distance between the center of the particle i and the center of mass of all the particles, and the mean radius $\bar{R} = 1/N\sum_{i=1}^{N} R_i$. We observe a sharp increase of the asphericity when the bubble starts to facet and a significant change of slope when inward buckling is observed [Fig. 2(b)].

We next calculate the pressure difference ΔP, using an algorithm in SE, between the bubble and its surroundings as a function of the reduced volume [Fig. 2(b)]. Unlike a normal bubble, where ΔP is a monotonically increasing function for decreasing reduced volume [Fig. 2(b)], ΔP of an armored bubble becomes a decreasing function at $(V/V_p)_{c1}$ and eventually reaches zero at $(V/V_p)_{c2}$. These results qualitatively agree with the shape of the experimen-

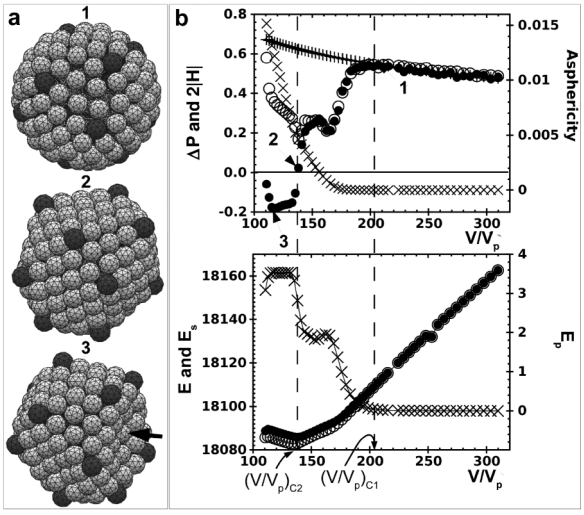

FIG. 2. (a) Simulated bubble shapes obtained for V/V_p equal to (1) 203, (2) 138, and (3) 120. The darker particles represent fivefold disclinations. The arrow indicates the facet which has buckled inward. (b) Top graph. Left vertical axis: (●) Laplace pressure, ΔP, vs V/V_p of the armored bubble. (+) For comparison, ΔP of a bubble without particles is shown. (○) 2 times the absolute value of the fluid-fluid interface mean curvature, $2|H|$, vs V/V_p. Right vertical axis: (×) asphericity of the armored bubble vs V/V_p. Bottom graph. Left vertical axis: (●) the surface energy E_S of the fluid-fluid interface and (○) the total energy E of the armored bubble vs V/V_p. Right vertical axis: (×) total repulsive energy E_P between particles vs V/V_p.

tally measured pressure curve of millimeter-size particle-covered oil droplets [19]. Figure 2(b) demonstrates the correlation between ΔP and the asphericity. Since the particles are held by the interface, this correlation suggests that the actual gas-liquid interface is being deformed as the volume is decreased. Indeed, the absolute value of the mean curvature $|H|$ of the gas-liquid interface follows exactly the variation of ΔP [except near $(V/V_p)_{c2}$, as SE gives only $|H|$]. It is thus clear that the vanishing of ΔP is due to the decrease of mean curvature of the gas-liquid interface towards zero.

Furthermore, we observe that the slope of the pressure-volume curve becomes positive at $(V/V_p)_{c1}$, i.e., $d\Delta P/dV > 0$, which is a requirement for stability [13]. For gas-saturated solutions, as considered in our experiments, ΔP also has to vanish to ensure mechanical equilibrium. However, more generally chemical potentials must be equal on either side of the interface [26], which can be satisfied with $\Delta P \neq 0$. Thus, in the cases of a supersaturated liquid, the bubble may stabilize at intermediate stages of faceting provided that the reduced volume is less than $(V/V_p)_{c1}$ (the limit being almost no faceting), while in moderately undersaturated solutions an armored bubble should stabilize with a buckled shape.

In order to check the stability in terms of energy, we calculate the total energy E, defined as the sum of the total surface energies E_S of all of the interfaces and the total repulsive energy E_P between the particles as a function of the reduced volume [Fig. 2(b)]. All energies are normalized by γL^2, where $L = V_p^{1/3} = (4\pi/3)^{1/3} a$. For comparison both E_S and E_P are plotted in Fig. 2(b). We observe that E and E_S change slopes as the particles start interacting, reaching a local minimum at the faceted shape when the particle interactions are the largest. Inward buckling of the facets [Fig. 2(a)3] corresponds to a local increase of E in the energy landscape. Thus, the local minimum is a metastable equilibrium.

The peculiar "kink" that the E_P curve exhibits during volume reduction [Fig. 2(b)] can be traced directly to the packing of the particles on the bubble surface. As the particles are pushed together during volume reduction, the 12 fivefold disclinations serve as the vertices of buckling [dark particles in Fig. 2(a)] and are pushed away from the center of the bubble. The increased distance slightly reduces E_P. This kink in E_P also leads to the kink in the $|H|$ and ΔP curves.

It appears that the configuration of the gas-liquid interface is intimately linked to the stability of the armored bubble. We thus sought to characterize the evolution of the gas-liquid interface whose shape can be fully specified by the local variation of the mean curvature H and the Gaussian curvature G. Obtaining accurate local numerical values of G for all simulated reduced volumes through SE proved impossible at the level of refinement of our surface due to numerical errors. Thus, we chose four representative stages in the evolution of the bubble and systematically refined the triangulation of the interface to reduce numerical noise. The spatial distributions of H and G were then determined with Matlab using algorithms for H [27] and G [28]. Representative images of the interface at approximately $(V/V_p)_{c2}$ are reported in a color-coded scheme in Fig. 3(a) and 3(b). Away from the particle contact lines the mean curvature H is very nearly constant, as expected on thermodynamic grounds and close to zero; G has a natural distribution since the Gaussian curvature need not be constant.

Despite the high level of refinement, it is apparent that there is still some dispersion in H (and in G as well), whose origins are (i) difficulty in numerical calculations near contact lines and (ii) errors associated with the triangulation valence around the vertices, which can be amplified during the determination of G [29]. Nevertheless, we can draw some conclusions about the global evolution of the surface curvatures. Indeed, a pair of values (H_i, G_i) is associated with each vertex defining the interface. To characterize the global nature of the interface, we calculate the number density of vertices whose curvatures range $[H, H + 0.03]$ and $[G, G + 0.03]$. We report in Figs. 3(c)–3(f) the plots of the contour maps of this binning of the $H - G$ space; shading corresponds to the number density of points. As a guide, a sphere would correspond to a parabola ($G = H^2$) in these plots and the

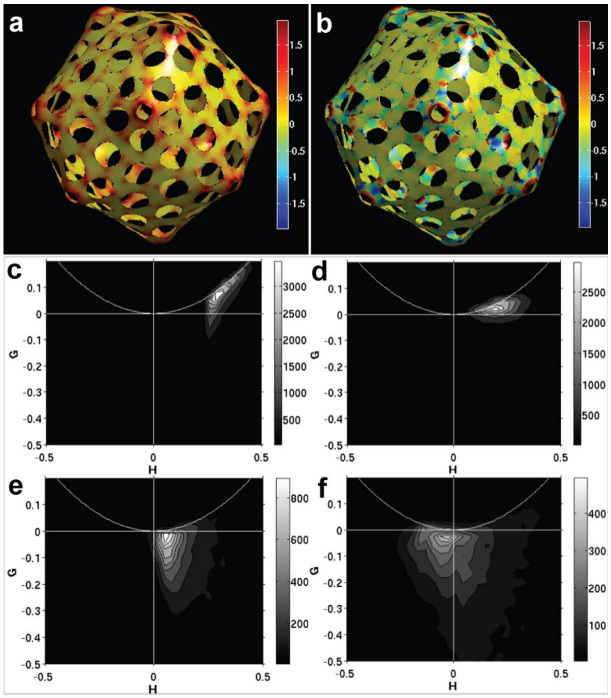

FIG. 3 (color online). Interfacial distributions of (a) the mean curvature H and (b) the Gaussian curvature G, for $V/V_p = 138.1$, which is close to $(V/V_p)_{c2}$. 2D histogram of the number of vertices of the interface whose curvatures range between $[H, H + 0.03]$ and $[G, G + 0.03]$ obtained for $V/V_p =$ (c) 253, (d) 162.3, (e) 138.1, and (f) 117.5. Total number of vertices 63 016.

origin (0, 0) corresponds to a planar interface. At large reduced volumes, when the particles are not interacting, the distribution of points is concentrated on the parabola, where both H and G are positive [Fig. 3(c)]. Then, for decreasing values of reduced volume, the center of the distribution shift towards zero in the H direction, while in the G direction it becomes negative. These results indicate a saddle-shape deformation of much of the interface as the volume is reduced.

The deformation of the interface is a consequence of Newton's third law, e.g., [13]. The repulsive interactions produce an outward normal force on each particle, because of their confinement on a closed surface. This outward force must be balanced by an inward saddle-shaped deformation of the fluid-fluid interface. This reactive deformation of the interface, which is required for mechanical equilibrium at each volume reduction, leads to a reduction in the Laplace pressure. We emphasize that this saddle-shaped deformation should appear on any initially spherical fluid-fluid interface carrying repulsive particles, as soon as the particles are close enough to interact. The details of the interparticle repulsive force are not relevant for this argument, the limiting case being that of a hard sphere repulsion between the particles, where the interface deviates from spherical only when the particles enter into contact.

In conclusion, we have shown that armored bubbles can adopt stable faceted shapes as gas dissolves into the surrounding liquid. These shapes are part of a continuous transition as a function of the ratio of the particle to bubble radius from clusters ($a/R \approx 1$) [21], to facets ($a/R \approx 0.1$), to crumpled shapes ($a/R \ll 0.1$) [1]. Through simulations we have demonstrated that the faceted state is a minimum energy configuration characterized by a mostly saddle-shaped gas-liquid interface with zero mean curvature. This minimum is also marked by the vanishing of the Laplace overpressure ΔP, and $d\Delta P/dV > 0$, which provides stability against dissolution. We expect these results to be robust for the crumpled shapes characterized by smaller particle to bubble radius ratios. The results we obtained in this study should also be applicable to describe the interface and behavior of liquid-liquid systems.

We thank the Harvard MRSEC (No. DMR-0213805) and Unilever Research for support and D. Gregory and R. S. Subramanian for helpful conversations. S. H. K. and S. M. Y. were supported by the Creative Research Initiative Program of MOST/KOSEF and the BK21 program. We thank E. Lauga for help with SE and an anonymous referee for helpful comments.

*Present address: Laboratoire des Colloïdes, Verres et Nanomatériaux, UMR5587, CC26, UMII, 34095 Montpellier Cedex 5, France.
abkarian@lcvn.univ-montp2.fr
†has@seas.harvard.edu

[1] W. Ramsden, Proc. R. Soc. London **72**, 156 (1903).
[2] B. Johnson and R. Cooke, Science **213**, 209 (1981).
[3] Z. Du, M. Bilbao-Montoya, B. Binks, E. Dickinson, R. Ettelaie, and B. Murray, Langmuir **19**, 3106 (2003).
[4] E. Dickinson, R. Ettelaie, T. Kostakis, and B. Murray, Langmuir **20**, 8517 (2004).
[5] R. Alargova, D. Warhadpande, V. Paunov, and O. Velev, Langmuir **20**, 10 371 (2004).
[6] B. Binks and T. Horozov, Angew. Chem. **44**, 3722 (2005).
[7] E. Schutt, D. Klein, R. Mattrey, and J. Reiss, Angew. Chem. **42**, 3218 (2003).
[8] P. Krachelsvky and K. Nagayama, *Particles at Fluid Interfaces and Membranes* (Elsevier Science, Amsterdam, 2001).
[9] A. Adamson and A. Gast, *Physical Chemistry of Surfaces* (Wiley-Interscience, New York, 1997), 6th ed.
[10] B. Gibbs, S. K. I. Alli, and C. Mulligan, International Journal of Food Sciences and Nutrition **50**, 213 (1999).
[11] J. Hilden and K. Trumble, J. Colloid Interface Sci. **267**, 463 (2003).
[12] R. Subramanian, R. Larsen, and H. Stone, Langmuir **21**, 4526 (2005).
[13] S. Kam and W. Rossen, J. Colloid Interface Sci. **213**, 329 (1999).
[14] A. B. Subramaniam, C. Méjean, M. Abkarian, and H. Stone, Langmuir **22**, 5986 (2006).
[15] See EPAPS Document No. E-PRLTAO-99-040741 for a few details that are not described in the text. For more information on EPAPS, see http://www.aip.org/pubservs/epaps.html.
[16] A. Bausch, M. Bowick, A. Cacciuto, A. Dinsmore, M. Hsu, D. Nelson, M. Nikolaides, A. Travesset, and D. Weitz, Science **299**, 1716 (2003).
[17] A. B. Subramaniam, M. Abkarian, and H. Stone, Nat. Mater. **4**, 553 (2005).
[18] A. B. Subramaniam, M. Abkarian, L. Mahadevan, and H. Stone, Nature (London) **438**, 930 (2005).
[19] H. Xu, S. Melle, K. Golemanov, and G. Fuller, Langmuir **21**, 10 016 (2005).
[20] K. Stratford, R. Adhikari, I. Pagonabarraga, J.-C. Desplat, and M. Cates, Science **309**, 2198 (2005).
[21] V. Manoharan, M. Elsesser, and D. Pine, Science **301**, 483 (2003).
[22] E. Lauga and M. Brenner, Phys. Rev. Lett. **93**, 238301 (2004).
[23] K. Brakke, Exp. Math. **1**, 141 (1992).
[24] A. B. Subramaniam, M. Abkarian, L. Mahadevan, and H. Stone, Langmuir **22**, 10 204 (2006).
[25] J. Lidmar, L. Mirny, and D. Nelson, Phys. Rev. E **68**, 051910 (2003).
[26] E. Guggenheim, *Thermodynamics: An Advanced Treatment for Chemists and Physicists* (North-Holland, Amsterdam, 1967), 4th ed.
[27] M. Meyer, M. Desbrun, P. Schröder, and A. H. Bartr, *Discrete Differential-Geometry Operators for Triangulated 2-Manifolds*, in Visualization and Mathematics III, edited by H.-C. Hege and K. Polthier (Springer-Verlag, Heidelberg, 2002).
[28] J. Goldfeather and V. Interrante, ACM Transactions on Graphics **23**, 45 (2004).
[29] V. Borrelli, F. Cazals, and J.-M. Morvan, Comput. Aided Geom. Des. **20**, 319 (2003).